Physics of Fluids, Volume 36, Issue 2, February 2024, Article number 027136
DOI:10.1063/5.0190630

Wave-assisted propulsion: an experimental study on traveling ships

ChunYin Chan,[1, a)] Junxian Wang,[1, a)] Liang Yang,[1] and Jun Zang[2]
[1)]*Division of Energy and Sustainability, School of Water, Energy and Environment (SWEE), Cranfield University, Bedford, MK43 0AL, UK*
[2)]*Department of Architecture & Civil Engineering, University of Bath, Bath, BA2 7AY, UK*

(*Electronic mail: liang.yang@cranfield.ac.uk)

(Dated: 11 March 2024)

A submerged hydrofoil interacting with incoming waves produces combined heaving and pitching motion, facilitating the conversion of wave energy into thrust. When the foil is attached to the ship hull, the generated 'green' power from wave energy could assist the ship's propulsion system and significantly reduce fuel costs. This study experimentally assesses thrust generation from a fixed mid-hull foil by comparing towing force at different wave and traveling speeds. The optimal mid-hull foil demonstrates a fuel cost reduction ranging from 10.3% to 20.4% at diverse traveling speed and wave parameters. Thrust generation increases at higher traveling speeds. Additionally, this study mathematically describes the hydrofoil motion with an outer pivot, which better suits the ship-foil model. This study then introduces a Strouhal number ($St_{A,S}$) specifically for the ship-foil model, considering ship travel, ship response, and the hydrofoil's rotation around its outer pivot.

I. INTRODUCTION

Taking inspiration from the moments of flying birds and swimming fishes, a foil-shaped body can generate thrust through its flapping motion[1], presenting a promising approach for an energy-efficient propulsion system. The submerged hydrofoil undergoes a flapping motion (heave and pitch) due to the wave excitation, which is a process that achieves the wave energy harnessing and the conversion into forward thrust[2,3]. Consequently, the hydrofoil can be affixed beneath a ship's hull to either replace or complement the ship's original propulsion system[4]. The technology of hydrofoils finds widespread application in unmanned surface vehicles (USVs)[5], including wave gliders[6,7]. Additionally, the flapping response of the hydrofoil can be harnessed to generate electricity, functioning as a wave energy converter (WEC)[8], and this leads to recent exploration of hydrofoil's hybrid application[9,10].

The foil attachment contributes to the reduction of ship dynamic response (e.g., pitch motion), ship resistance, and further fuel costs. Foils that fixed to ships[11–15] achieve flapping motion straightforwardly from ships' dynamic interaction with waves. Bøckmann and Steen[11] conducted experimental tests on a ship with two fixed bow foils, reporting a substantial reduction of up to 17% in ship resistance, as well as 32% and 25% reductions in heave and pitch. A spring-loaded foil[16–18] employs springs to provide the restoring force and has revealed superb energy extraction performance[19]. Bowker and Townsend[4] carried out experiments on a free-running ship with a spring-loaded bow foil, demonstrating a 50% reduction in provided power for regular waves and a 12% reduction for irregular waves. Foils can also be actively flapped[14,20], serving as thrusters. Huang et al.[21] experimentally compared the fixed bow foil and active pitching foil using a free-running ship, concluding an 11.86% speed improvement and an 18.9% energy saving for the active pitching foil at proper wave conditions. The foil can be designed as retractable[22–24], retracting in calm water and deploying in waves, to facilitate fuel savings[22]. The attached foil can also be designed to passively adjust[25] angle of attack, to enhance wave energy conversion and mitigate ship pitch motion.

Based on the aforementioned research background, foils are typically fixed to the ends of ships (bow or stern) due to higher ship response near these locations. The study about foils underneath the mid-hull is limited[13,14], making it a topic worthy of investigation. The hydrofoil's pivot location in previous studies[26–29], within the foil's geometric shape, is not suitable for the 'ship-foil' model. Therefore, studies on its pivot location should explore the position outside the foil's geometry. Additionally, parametric studies on 'foil only' reveal that the foil shape[30,31], freestream velocity (related to the effective angle of attack[32,33]), and wave parameters[34] affect thrust generation, providing controlling variables for studying the fixed mid-hull foil.

Consequently, the present study experimentally tested a ship model with a fixed mid-hull foil in regular waves, in comparison to a 'ship-only' model. The ship was towed against regular waves, and both the towing force and the model's pitch motion were collected to evaluate the thrust generated by the hydrofoil. Through this series of experiments, a comparison of the generated thrust was made to reveal the optimal hydrofoil type out of five different models, followed by an exploration of the impacts of different towing speeds and wave conditions. This study then mathematically described the hydrofoil's motion with an outer pivot and introduced a Strouhal number ($St_{A,S}$) for the ship-foil model. This Strouhal number accounts for the superposed motion of the traveling ship, its response, and the rotation around the outer pivot, providing a more accurate description of the ship-foil model. However, it is important to note that the Strouhal number calculated by the introduced $St_{A,S}$ represents a range value, effectively indicating a certain limitation.

[a)]These authors contributed equally to this work.

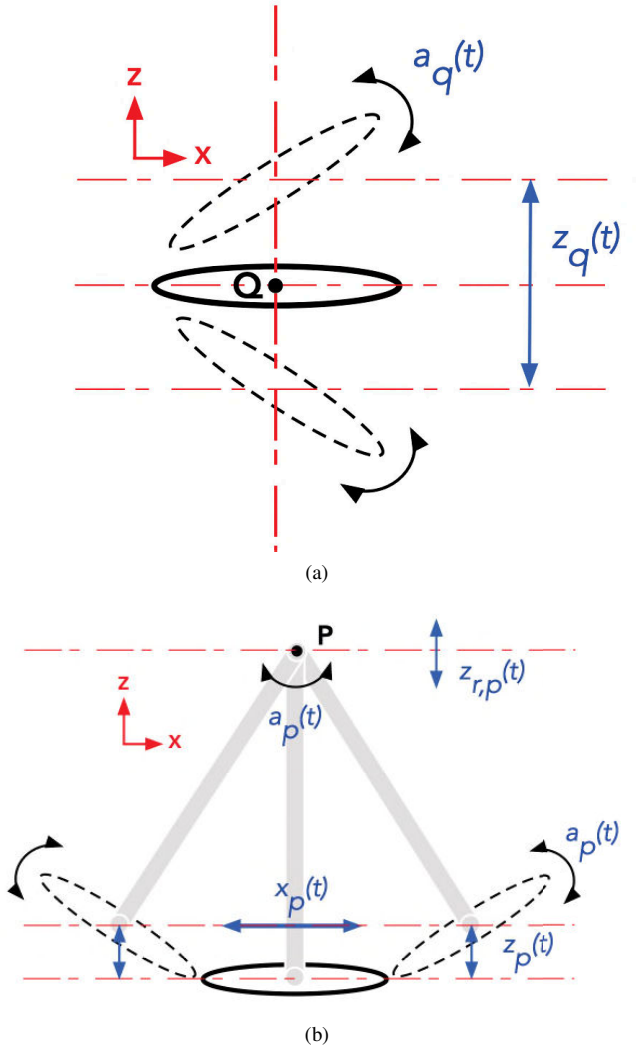

FIG. 1. Schematic sketch of flapping hydrofoil motion for inside pivot (a) and outside pivot (b); the ellipse stands for the hydrofoil.

II. METHODOLOGY

A. Hydrofoil motion

The normal definition of a hydrofoil's flapping motion involves a combined heaving and pitching motion, corresponding to $z_q(t)$ and $a_q(t)$ as plotted in figure 1a. It can be mathematically expressed as two coupled sinusoidal paths at an identical frequency with a certain phase difference, as given by:

$$z_q(t) = A_q \sin(\omega t), \tag{1}$$

$$a_q(t) = B_q \sin(\omega t + \alpha), \tag{2}$$

where A_q, B_q are heaving amplitude, pitching amplitude; ω and α denote the motion angular frequency and phase difference.

It is worth noting that, according to the flapping motion definition in figure 1a, the pivot point (Q) is within the hydrofoil geometric outline. However, when fixing the hydrofoil underneath the ship's hull, the ship's scale is much larger than that of the hydrofoil. The flapping motion defined by equation 1, 2 is not applicable owing to the pivot point being out of the hydrofoil geometry. As a result, the present study introduces another definition of flapping motion with an outside pivot, as shown in figure 1b. For simplification, the pivot point (P) is specified right above the hydrofoil's central point at a distance defined as l_0 (i.e., the grey rod in figure 1b). A coupled sinusoidal motion is prescribed at the pivot point P, and the expression is given as:

$$z_{r,p}(t) = A_p \cos(\omega t), \tag{3}$$

$$a_p(t) = B_p \cos(\omega t + \alpha), \tag{4}$$

where $z_{r,p}(t)$, $a_p(t)$ represent the heaving and pitching motion of P; A_p and B_p denote the corresponding heaving and pitching amplitudes. Concerning the hydrofoil, its pitching motion can also be expressed as $a_p(t)$ in equation 4. Additionally, its rotation around P decomposes into two motion components: a vertical oscillation and a horizontal oscillation. Consequently, its surge motion $x_p(t)$ and heaving motion $z_p(t)$ are given by:

$$z_p(t) = l_0(1 - \cos(\omega t + \alpha)) + z_{r,p}(t), \tag{5}$$

$$x_p(t) = l_0 \sin(\omega t + \alpha), \tag{6}$$

where l_0 represents the distance between P and the hydrofoil centre. $x_p(t)$ denotes pure rotation-induced surge, and $z_p(t)$ is a combined motion, including the rotation-induced heave and pivot (P) heave.

Comparing the two types of hydrofoil flapping discussed above, a notable difference arises. The hydrofoil with an outside pivot (see figure 1b) exhibits additional heave and surge motion originating from its rotation around pivot location P. While the coupled motion of $z_q(t)$ and $a_q(t)$ for the hydrofoil with an inside pivot generates horizontal thrust, the outside pivot hydrofoil's coupled motion of $[z_p(t), a_p(t)]$ and $[x_p(t), a_p(t)]$ results in both horizontal and vertical thrust. Consequently, the hydrofoil fixed to the ship aligns better with the motion described in figure 1b, leading to the generation of both vertical and horizontal thrust.

The experimental model employed in this study is a ship with a mid-hull fixed hydrofoil, as illustrated in figure 2. The large scale difference between the ship and the attached foil results in an outside pivot for the hydrofoil's flapping motion, aligning with the concept depicted in figure 1b. Consequently, the hydrofoil's dynamic motion can be calculated by combining its rotation around point P with the wave-excitation response centered on P.

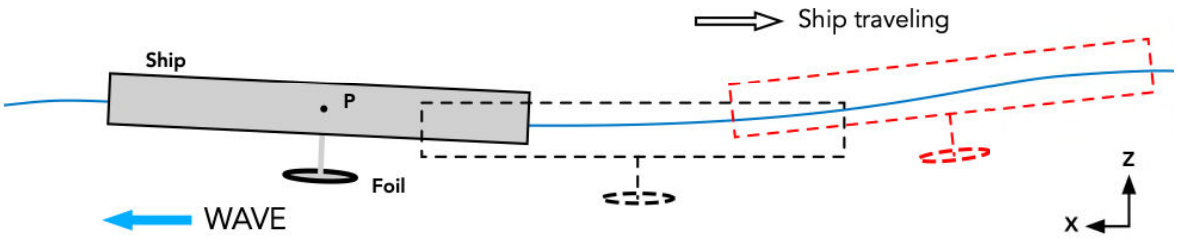

FIG. 2. Schematic sketch of ship motion in waves.

B. Experimental setup

The experiments investigating ship-foil interaction with waves were conducted in the open circulation ocean wave tank at Cranfield University[18]. The tank is equipped with three powerful paddles situated at one end, enabling the generation of regular waves with a maximum height of 0.28 m and a frequency range of 0.1 Hz to 1.1 Hz. These waves cover both deep-water and shallow-water conditions, with most being intermediate wave. To minimize wave reflection, an artificial beach is installed at the other end of the tank. Additionally, a towing system above the wave tank enables the towing of floating objects with predefined acceleration, velocity and positions within specified limits to study their dynamic responses. The configuration and working limits of the wave tank and towing system are detailed in table I.

TABLE I. Parameters of ocean wave tank and towing system.

Items	Properties	Value
1	Dimension (Length*Width*Height)	30 m * 1.5 m * 1.8 m
2	Water Depth	1.5 m
3	Range of Working Frequency	0.1 Hz - 1.1 Hz
4	Maximum Wave Height	0.28 m
5	Maximum Towing Velocity	3.5 m/s
6	Max Towing Carriage Payload	75 kg
7	Max Towing Carriage Drag	200 N

The experimental setup for this study is illustrated in detail in figure 3. The ship model used in the experiments is a scaled-down Volvo Ocean Race (VOR) 70 shape model, approximately 1.077m in length (l_S), and featuring a stratification surface with carbon fibers. Approval for the model's usage in the experiments has been granted by the Process Systems Engineering (PSE) laboratory of Cranfield University specifically for this study. The hydrofoil model is fixed underneath the middle of the ship's hull at a distance of 0.15 m (d_H) between ship's bottom and the chord line of the foil. To maintain ship's traveling direction, a stabilizing rudder (an aluminium plate) is positioned at the ship's stern. Two three-dimensional (3D) printing components, marked as green blocks in figure 3, are attached to the ship's bottom and stern to support the foil and rudder, respectively. Additionally, three 0.335 kg weight balances are located inside the ship model for further stabilization. The towing carriage, which travels freely along rails over the wave tank, is connected to the ship's bow using fishing lines. Four low-stiffness tension springs with a stiffness of 48 N/m are connected in series between the fishing lines to ensure the taut status of the fishing lines during the ship's dynamic response throughout the experiments.

TABLE II. Parameters of hydrofoil models.

Model	NACA[a] Type	Chord c (m)	Span d (m)	Pivot ratio	Projected area (m^2)
1	0030	0.15	0.23	1:2	0.01035
2	0030	0.15	0.23	3:2	0.01035
3	0030	0.10	0.23	1:2	0.0069
4	0030	0.10	0.23	3:2	0.0069
5	0012	0.15	0.23	1:2	0.00414

[a] NACA: National Advisory Committee for Aeronautics

A total of 5 different sets of three-dimensional (3D) printed hydrofoils (material: polylactic acid, PLA) were prepared for the experiments, varying in hydrofoil type, scale, and pivot location, as outlined in table II. The pivot ratio is defined as the ratio of the distance from the pivot point (P_f) to the leading edge to the distance from the pivot point to the trailing edge. For the initialization of all hydrofoil models, the chord line, which connects leading edge and trailing edge, is parallel to the still water surface. the draft of the hydrofoil is approximately 0.15 m.

C. Experimental arrangement and data processing

The Greater Ekofisk area in the North Sea has been selected as a reference for obtaining specific water parameters, with a wave height of 14 m and a wave period of 16 s[35]. To adapt these parameters to the capabilities of the ocean wave tank, a scale factor of 100 was chosen. Consequently, the scaled-down reference regular wave parameters are 0.07 m and 0.625 Hz for wave amplitude (A_W) and frequency (f_W), respectively. The reference towing speed (u_T) of the towing carriage is 0.55 m/s, and the experimental water depth (H) is maintained at 1.5 m.

The present experiments consists of three stages: determining the optimal hydrofoil type, exploring the effect of towing

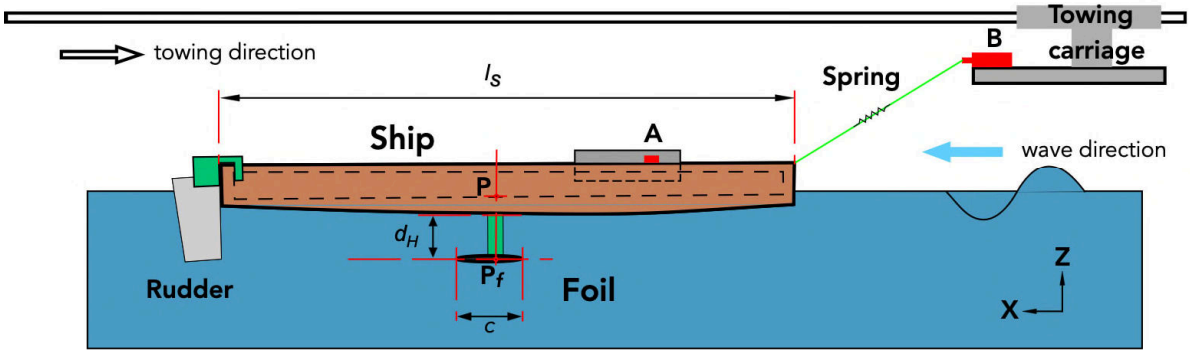

FIG. 3. Schematic sketch about experimental setup.

TABLE III. Summary of working conditions at various towing speeds (u_T).

Case	A_W (m)	f_W (Hz)	u_T (m/s)	Foil model
1	0.07	0.625	0.55	NF[a], Model 1-5
2	0.07	0.625	0.5	NF, Model 5
3	0.07	0.625	0.45	NF, Model 5
4	0.07	0.625	0.4	NF, Model 5
5	0.07	0.625	0.35	NF, Model 5

[a] NF: No Foil

TABLE IV. Summary of working conditions in diverse waves.

Case	A_W (m)	f_W (Hz)	u_T (m/s)	Foil model
6	0.055	0.709	0.55	NF, Model 5
7	0.0625	0.664	0.55	NF, Model 5
8	0.0675	0.637	0.55	NF, Model 5
9	0.0725	0.613	0.55	NF, Model 5
10	0.0775	0.591	0.55	NF, Model 5
11	0.085	0.561	0.55	NF, Model 5

speed, and investigating the impact of wave parameters. In the first stage, five different hydrofoil models (see table II) were fixed underneath theship's mid-hull and tested successively under reference wave conditions (0.07 m A_W, 0.625 Hz f_W), and a towing speed (u_T) of 0.55 m/s. The corresponding results were compared to those of the ship without an attached foil (indicated as "NF" shown in table III, IV), leading to the identification of the optimal hydrofoil model (Model 5). The subsequent experiments employed Model 5 under reference regular waves and various towing speeds, as summarized in table III. The third stage explores the impact of different regular wave conditions using Model 5 with a fixed towing speed at 0.55 m/s. To achieve this, the wave conditions were varied by changing the wave scale, as characterized by different amplitudes and frequencies (see the cases in table IV), while maintaining a constant wave steepness, S_W, that is defined here as:

$$S_W = kA_W, \tag{7}$$

where A_W is the wave amplitude and k is the wavenumber obtained by the linear dispersion relation (associated with the depth of water and the wave frequency). Based on equation 7, the calculated values of the wave steepness for waves presented in table III and IV remain at 0.11. The reason of employing a constant wave steepness across all experiments is to keep the wave nonlineairty constant and avoid potential breaking events[36], so that the identical maximum flapping angle of the foil is achieved.

Ship performance, including ship resistance and pitch motion, was comprehensively evaluated using data collected from the Vernier load cell and the WitMotion inclinometer/accelerometer, with detailed specifications provided in table V. The data was collected and processed using software paired with sensors. The Vernier load cell is mounted onto the towing carriage, where the fishing line attached to the ship bow is connected to the hook at the bottom of the load cell (marked as red Block B in figure 3). The load cell is horizontally placed throughout the experiments, and its sampling frequency was set to 50 Hz. During the experiments, the recorded force of ship with and without foil is termed $F_{s,f}$ and F_s. The force difference between with ($F_{s,f}$) and without (F_s) the attached foil stands for the generated thrust (F_{thrust}) due to foil flapping, as expressed in equations 8. Besides, the effectiveness (R_{eff}) can be defined in equation 9 to evaluate the total reduction in fuel cost. The WitMotion sensor in the present project is responsible for measuring ship pitch angle variation. It is mounted on top of the compartment, situated close to the middle of the ship horizontally (marked as red Block A in figure 3). It is worth noting that although the inclinometer is not positioned at the centre of rotation (CoR), the measured pitch angle can accurately reflect the pitch motion of foil, as well as the ship.

$$F_{s,f} = F_s - F_{thrust}, \tag{8}$$

$$R_{eff} = \frac{F_{thrust}}{F_s}. \tag{9}$$

TABLE V. Details of load cell and inclinometer/accelerometer.

Items	Properties	Value
	Load cell	
1	Force range	± 50 N
2	Sampling rate (max)	1000 samples/s
	Inclinometer/Accelerometer	
1	Acceleration range	± 16 g
2	Acceleration resolution	0.005 g
3	Angle range	± 180° (X, Z), ± 90° (Y)
4	Angle accuracy (X, Y)	0.05° (Static), 0.1° (Dynamic)

III. RESULTS AND DISCUSSION

Upon completing the preparation procedures, experiments were carried out for the defined cases. During the experiments, the towing carriage moved along the rail at the prescribed towing speed, pulling the ship model against the regular waves. A representative film capture is presented in figure 4. In the first stage, five different hydrofoil models were successively attached to the ship mid-hull and tested at the reference wave (A_W = 0.07 m, f_W = 0.625 Hz), reference towing speed 0.55 m/s. The comparison of effectiveness (R_{eff}) of different hydrofoils identified Model 5 (NACA0012) as the optimal hydrofoil. Subsequently, towing force and generated thrust (F_{thrust}) were found to increase as the towing speed climbed from 0.35 m/s to 0.55 m/s. In the third stage, diverse waves (A_W = 0.055 to 0.085 m, f_W = 0.709 to 0.561 Hz) with a constant wave steepness concluded similar thrust generation. Furthermore, based on the hydrofoil's motion with the outer pivot, the Strouhal number ($St_{A,S}$) for ship-foil model was introduced, considering the integration of ship traveling, ship response, and foil rotation. Testing for each case was repeated 2 to 4 times which ensure data reliability.

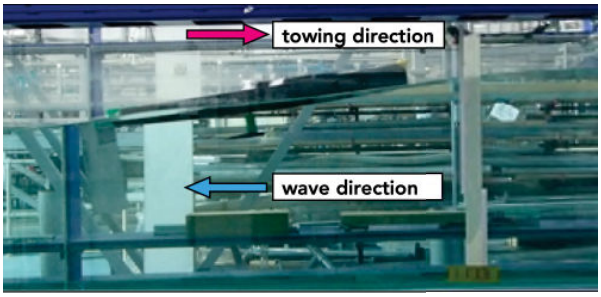

FIG. 4. A film capture of experiment with hydrofoil Model 5 (NACA0012) at reference wave (A_W 0.07 m, f_W 0.625 Hz), towing speed 0.55 m/s.

A. Thrust generation

The primary objective of this subsection is to compare the ship performance using five different hydrofoil models under reference wave and towing speed conditions, ultimately determining the optimal hydrofoil. The recorded time series of force, i.e., F_s, $F_{s,f}$, oscillated as the ship traveled through the crest and trough of the wave propagation. In comparison to Model 1-4 (NACA0030 series), the results from Model 5 (NACA0012) demonstrated a notable capability to produce thrust for the ship through wave energy harnessing. This phenomenon can be attributed to the difference in geometry, where the NACA0030 type has a higher projected area than that of NACA0012 as shown in table II. Consequently, the NACA0030 hydrofoil induces larger drag, which neutralizes the generated thrust from hydrofoil's flapping motion in the present study. As a result, Model 5 (NACA0012) was chosen as the optimal hydrofoil, and an analysis of the corresponding recorded force is provided in this subsection. A 10-second time-frame from a single test was extracted for time-averaging, and each case was repeated to three times for reliable averaged output.

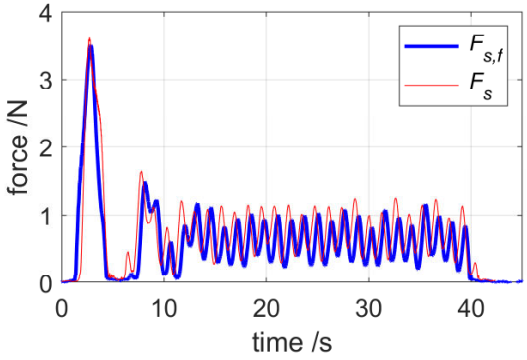

FIG. 5. Recorded force for representative cases with Model 5 (NACA0012) hydrofoil and without hydrofoil at reference wave (A_W 0.07 m, f_W 0.625 Hz), towing speed 0.55 m/s.

TABLE VI. Summary of all tests for Model 5 (NACA0012) at reference wave, reference towing speed.

	F_s (N)	$F_{s,f}$ (N)	F_{thrust} (N)	R_{eff}
Test 1	0.75133	0.63672		
Test 2	0.76400	0.61222		
Test 3	0.78499	0.61619		
Total Average	0.76677	0.62171	0.14506	18.9%

The recorded forces for the ship with ($F_{s,f}$) and without (F_s) the NACA0012 foil at the reference wave and towing speed are compared and illustrated in figure 5, where they exhibit similar oscillation shapes. In the initial part (e.g., 0 to 10 seconds), the launch of the carriage and its acceleration lead to larger and unstable forces. Similarly, as the towing carriage gradually slows down (40 seconds and beyond), the force decreases to zero. In the stabilised region in between, the force fluctuates at a stable frequency and amplitude. A straightforward observation from the oscillated value is that the recorded force for the ship with the NACA0012 is smaller than that from the ship-only testing. This difference directly confirms that the flapping NACA0012 foil, due to wave excitation, generates a notable thrust (F_{thrust}), which partially counterbalance

the ship resistance. The 10-second averaged forces from three tests for the ship with/without the NACA0012 foil are summarized in table VI. Notably, the averaged recorded force for all trials with the NACA0012 is significantly lower than that of the ship-only trials. The total averaged generated thrust (F_{thrust}) from the hydrofoil is 0.14506 N, indicating an effectiveness of 18.9%. As a result, the thrust and its effectiveness demonstrate that the attachment of the NACA0012 to the ship mid-hull contributes to around an 18.9% reduction in overall fuel consumption.

B. Effect of towing speed and wave

As discussed in section III A, the NACA0012 hydrofoil generates satisfactory thrust for powering the ship. This subsection continues to investigate the impact of ship traveling speed and wave parameters by adopting the NACA0012 hydrofoil model. Towing speed of the carriage varies from 0.5 m/s to 0.35 m/s as shown in Case 2 to 5 in table III. Diverse wave amplitudes (0.055 - 0.085 m) and frequencies (0.709 - 0.561 Hz) are specified in table IV.

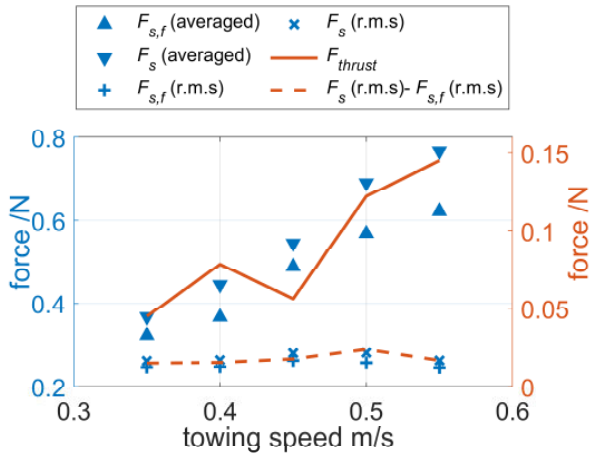

FIG. 6. Force comparison for Model 5 (NACA0012) in stabilised region for reference wave (A_W 0.07 m, f_W 0.625 Hz), diverse towing speed (0.35 - 0.55 m/s).

TABLE VII. Summary of Model 5 (NACA0012) at reference towing speed (0.55 m/s), diverse wave parameters.

Case	A_W (m)	f_W (Hz)	F_s (N)	$F_{s,f}$ (N)	F_{thrust} (N)
1	0.07	0.625	0.76677	0.62171	0.14506
6	0.055	0.709	1.07239	0.7696	0.30279
7	0.0625	0.664	0.73566	0.61677	0.11889
8	0.0675	0.637	0.75741	0.60271	0.1547
9	0.0725	0.613	0.76993	0.62979	0.14014
10	0.0775	0.591	0.87135	0.69779	0.17356
11	0.085	0.561	0.88894	0.74578	0.14316

As the ship, with/without NACA0012 foil, travels against the reference wave at towing speed ranging from 0.35 m/s to 0.55 m/s, the time-averaged and root-mean-square (r.m.s) value of the recorded force in the stabilised region are summarized in figure 6. At each towing speed, it is clear that the attachment of the NACA0012 foil results in a reduction in the averaged force, as well as the r.m.s value of force, indicating the reproducible finding that the generated thrust from hydrofoil partially counterbalances ship resistance, and the wave-induced hydrofoil's flapping motion reduces force fluctuation. It can also be observed that the force r.m.s value for with/without hydrofoil remains at a stable level, around 0.25, throughout the towing speed range, and the r.m.s difference for each speed also keeps stable. However, the averaged force for with/without foil significantly increases with the increase in towing speed, and the force difference represents the generated thrust (F_{thrust}), which also experiences a notable upward trend. The effectiveness (R_{eff}) ranges between 10.3% and 18.9% across all towing speeds. It should be noted that the carriage's towing speed aligns with the ship's traveling speed in calm water, as there is no involved vertical velocity component. In the present study, when applied to waves, the actual ship traveling speed should be a superposition of the towing speed and the wave's vertical speed, but changes in towing speed can also directly influence and evaluate the ship's traveling speed.

Subsequently, while maintaining the same wave steepness, varied wave parameters were tested and the corresponding results are presented in table VII. The extreme wave condition (case No. 6, A_W = 0.055 m, f_W = 0.709 Hz) resulted in the highest towing forces, possibly due to a significant increase in resistance. Additionally, the highest flapping frequency of the hydrofoil in Case No. 6 is considered to dominate and contribute to its highest thrust generation. The remaining cases (No. 1, 7 to 11) with variation in wave parameters resulted in steady force values for both with ($F_{s,f}$) and without (F_s) the NACA0012 hydrofoil, in the range of 0.60 to 0.75 N and 0.74 to 0.89 N, respectively. Thus, the generated thrust from the foil varies from 0.12 to 0.17 N for the remaining cases, accounting for a stable range of effectiveness from 16.1% to 20.4%. In general, it is concluded that the NACA0012 hydrofoil is capable of achieving a lower fuel consumption rate, despite of reductions in traveling speed and changes in wave parameters, enabling the ship to attain even better fuel efficiency.

C. Extension on Strouhal number

In the analysis of hydrofoils, the Strouhal number based on amplitude, referred to as St_A, is commonly used to characterise the transition from drag to thrust[37]. It is calculated by dividing the product of frequency (f) and amplitude (A) by velocity (u_∞)[1]. However, the motion of a hydrofoil fixed to a ship hull is complicated, as described in section II A, involving a superposition of ship traveling, wave response and rotation (outer pivot)-induced heaving and pitching. Consequently, the original definition of the Strouhal number (St_A) for a hydrofoil is not directly applicable and the complexity

of hydrofoil motion necessitates corrections to the terms mentioned above. As a result, this section introduces a Strouhal number ($St_{A,S}$) specifically for the hydrofoil fixed to a ship, taking into account the superimposed motion.

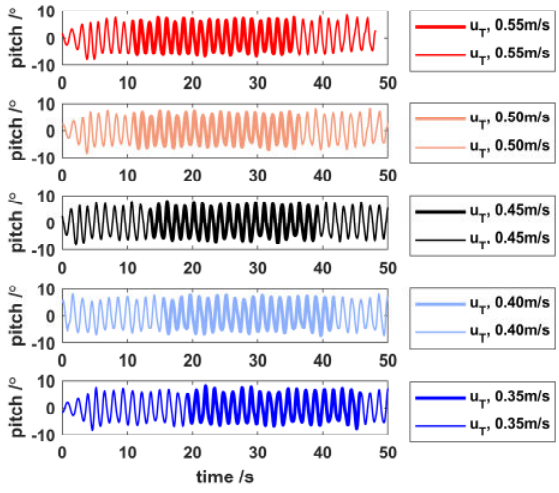

(a)

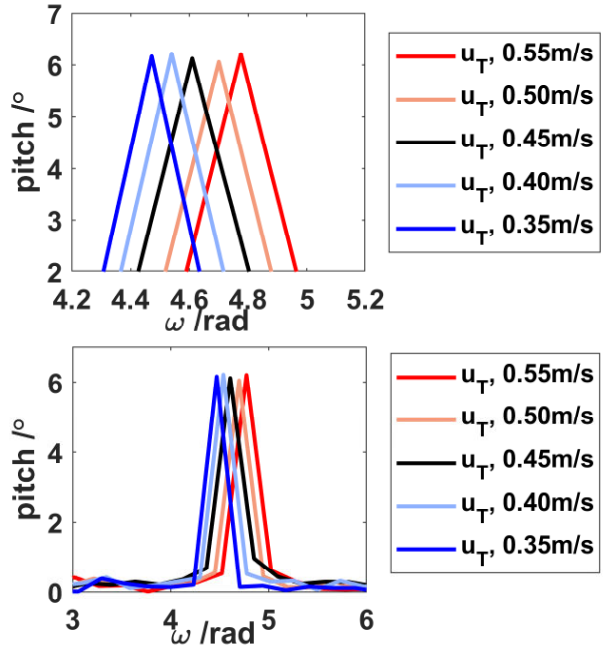

(b)

FIG. 7. Pitch variation (a) and pitch spectra (b) at reference wave, different towing speed (u_T). Pitch variation (a) contains time series (thin lines) and 20 selected cycles (bold lines). Angular frequencies (ω) are 4.775, 4.700, 4.609, 4.539, 4.471 corresponding traveling speed 0.55 to 0.35 m/s.

The time series of pitch variation of the traveling ship with the NACA0012 foil at the reference wave (A_W 0.07 m, f_W 0.625 Hz) and towing speeds (0.55 to 0.35 m/s) are displayed in figure 7a. A total of 20 pitch cycles (marked as bold lines in figure 7a) are selected to extract the corresponding spectra in figure 7b. The angular frequency (ω) at different towing speeds (0.55 to 0.35 m/s) varies, with values ranging from 4.775 to 4.471, indicating that the frequency strongly depends on the traveling speed. Therefore, the frequency (f_S) can be estimated based on ship traveling and wave propagation. The wave propagation speed (u_{wave}) is described as:

$$u_{wave} = f_W \lambda, \tag{10}$$

where f_W and λ are the wave frequency and wavelength. Set the reference system on the moving ship, the frequency differs due to traveling speed (u_T) and traveling direction. The correction of frequency (f_S) can be given in vector form as:

$$f_S = \frac{|\overrightarrow{u_{wave}} + \overrightarrow{u_T}|}{\lambda}, \tag{11}$$

by substituting the reference wave data (u_{wave} = 2.46 m/s, λ = 3.94 m) and towing speed (u_T = 0.55 to 0.35 m/s) into equation 11, the theoretical angular frequency ω_S (i.e., $2\pi f_S$) is 4.8, 4.720, 4.64, 4.561, 4.481, which is in agreement with the experimentally obtained values shown in figure 7b.

As described in equations 4 to 6, the foil's amplitude (A_S) in the present ship-foil model is a superposition of the pitching amplitude onto the ship's maximum heaving response (A_p). The corresponding expression is given by:

$$A_S = \sqrt{A_p^2 + (rc\sin(B_p))^2}, \tag{12}$$

where c and B_p stand for the chord length of the hydrofoil and the maximum flapping angle, respectively. The ratio r describes hydrofoil's connection location. The present experimental model fixed the rod to the middle of the hydrofoil, thus r is 0.5. The estimation of velocity ($u_{\infty,S}$) for the foil attaching to the ship is also a superposition of the ship traveling speed, rotation (outer pivot)-induced horizontal velocity component ($u_{r,x}$) and wave particle velocity at the foil position (u_x). According to airy wave theory, for a given wave, the water particle velocity (u_x, u_z) at a given vertical position (z_0) can be expressed as:

$$u_x(t) = 2\pi f_W A_W \frac{\cosh k(H+z_0)}{\sinh kH} \cos(kx_0 - 2\pi f_W t), \tag{13}$$

$$u_z(t) = 2\pi f_W A_W \frac{\sinh k(H+z_0)}{\sinh kH} \sin(kx_0 - 2\pi f_W t), \tag{14}$$

where A_W, f_W represent wave amplitude and wave frequency, respectively; k and H denote wavenumber and water depth, respectively. Typically, the orbit of a water particle in wave is elliptical. The corresponding path deforms into curves, as shown in figure 8, due to the superposition of the ship travel.

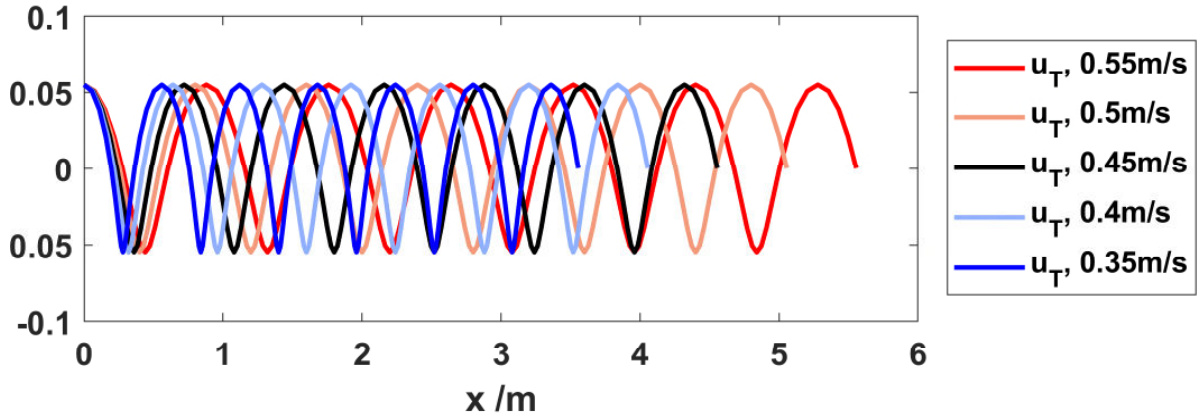

FIG. 8. Water particle (0.15m underneath free water surface) trajectory for reference wave with the superposition of diverse towing speed.

The rotation-induced speed ($u_{r,x}$) can be calculated according to figure 1b and equation 4:

$$u_{r,x}(t) = \dot{a_p}(t)\, l_0 \cos(a_p(t)), \tag{15}$$

where l_0 stands for the distance between outer pivot position and the hydrofoil.

$$St_{A,S} = \frac{f_S A_S}{u_{\infty,S}} = \frac{f_S A_S}{u_T \pm u_x(max) \pm u_{r,x}(peak)}. \tag{16}$$

The Strouhal number ($St_{A,S}$) specifically for the ship-foil model is put forward as expressed in equation 16. It is essential to note that the estimation of $St_{A,S}$ uses the maximum of u_x and the peak value of $u_{r,x}$ spectral. Consequently, the Strouhal number ($St_{A,S}$) can be estimated by substituting the obtained experimental data into equation 16. Data of a test at the reference wave (A_W 0.07 m, f_W 0.625 Hz) and towing speed (0.55 m/s) was utilized, and key parameters are provided in table VIII. f_S was theoretically calculated using equation 11, where θ is zero. A_p in the table was estimated by comparing the foil's heaving motion range and wave height in obtained film sequence. B_p is extracted from the pitch spectra shown in figure 7b. $u_x(max)$ was calculated from equation 13. Additionally, $u_{r,x}(peak)$ is obtained from the $u_{r,x}$ spectra. The $u_{r,x}$ time series can be post-processed using equation 15, where angular velocity of foil's pitch ($\dot{a_p}(t)$) for the present experiments was collected using the pitch sensor. The estimated range for the Strouhal number ($St_{A,S}$) is 0.044 to 0.15, as shown in table VIII.

TABLE VIII. Strouhal number ($St_{A,S}$) estimation for a testing case (Model 5, NACA0012) at reference wave (A_W 0.07 m, f_W 0.625 Hz), reference towing speed (u_T 0.55 m/s).

f_S	A_p	B_p	$u_x(max)$	$u_{r,x}(peak)$	$St_{A,S}$
0.764	0.048	6.21°	0.22	0.0787	0.044 - 0.15

IV. CONCLUSION

The flapping hydrofoil converts wave energy into thrust, and its attachment to the ship hull achieves significant reduction in fuel costs during ship travel in waves. This study experimentally tested the thrust generation performance of a mid-hull foil at different towing speeds and incoming wave conditions.

The results for the optimal mid-hull foil type (Model 5, NACA0012) at diverse speeds (0.35 to 0.55 m/s) and waves (A_W = 0.0625 to 0.085 m, f_W = 0.664 to 0.561 Hz) reveals a notable fuel saving (R_{eff}) in the range of 10.3% to 20.4%. The thrust generation increases with ship traveling speed. The results in terms of reducing fuel consumption provide valuable reference for hydrofoil application, especially the mid-hull foil. The Strouhal number ($St_{A,S}$) of the mid-hull foil were introduction and evaluated. The introducing of hydrofoil motion with outer pivot, as well as the Strouhal number ($St_{A,S}$) for ship-foil model, contributes to the following parametric study.

ACKNOWLEDGMENTS

This work has been supported by the Department for Transport's (DfT) Transport Research and Innovation Grants (TRIG2022): G-TRANSPORT: greening transportation of cargo ships via hybrid wave propulsion.

DECLARATION OF COMPETING INTEREST

The authors declare that they have no known competing financial interests or personal relationships that could have appeared to influence the work reported in this paper.

[1] X. Wu, X. T. Zhang, X. L. Tian, X. Li, and W. Y. Lu, "A review on fluid dynamics of flapping foils," Ocean Engineering **195**, 106712 (2020).
[2] J. Xing and L. Yang, "Wave devouring propulsion: An overview of flapping foil propulsion technology," Renewable and Sustainable Energy Reviews **184**, 113589 (2023).

[3] K. Rozhdestvensky and B. Zhao, "Recent advances in hydrodynamics of wing propulsive lifting systems for ships and underwater vehicles," Physics of Fluids **35** (2023), 10.1063/5.0169938.

[4] J. A. Bowker and N. C. Townsend, "Evaluation of bow foils on ship delivered power in waves using model tests," Applied Ocean Research **123**, 103148 (2022).

[5] Y. Li, W. Zhang, Y. Liao, Q. Jia, and Q. Jiang, "Multi-energy-system design and experimental research of natural-energy-driven unmanned surface vehicle," Ocean Engineering **240**, 109942 (2021).

[6] Z. Qi, M. Jiang, L. Jia, B. Zou, and J. Zhai, "The effect of mass ratio and damping coefficient on the propulsion performance of the semi-active flapping foil of the wave glider," Journal of Marine Science and Engineering **8**, 303 (2020).

[7] W.-Q. Wang, W. Li, Y. Yan, and J. Zhang, "Parametric study on the propulsion and energy harvesting performance of a pitching foil hanging under a wave glider," Renewable Energy **184**, 830–844 (2022).

[8] A. Arredondo-Galeana, W. Shi, G. Olbert, M. Scharf, A. Ermakov, J. V. Ringwood, and F. Brennan, "A methodology for the structural design of liftwec: A wave-bladed cyclorotor," in *The 14th European Wave and Tidal Energy Conference* (2021).

[9] J. A. Bowker, *Coupled dynamics of a flapping foil wave powered vessel*, Ph.D. thesis, University of Southampton (2018).

[10] Y. Zhang, X. Han, Y. Hu, X. Chen, Z. Li, F. Gao, and W. Chen, "Dual-function flapping hydrofoil: Energy capture and propulsion in ocean waves," Renewable Energy , 119956 (2024).

[11] E. Bøckmann and S. Steen, "Model test and simulation of a ship with wavefoils," Applied Ocean Research **57**, 8–18 (2016).

[12] R. McGregor and G. Thomson, "Sea trials of wave propulsion of a yacht using a flexible fin propeller," Renewable energy **10**, 335–338 (1997).

[13] K. A. Belibassakis and G. K. Politis, "Hydrodynamic performance of flapping wings for augmenting ship propulsion in waves," Ocean Engineering **72**, 227–240 (2013).

[14] K. Belibassakis and E. Filippas, "Ship propulsion in waves by actively controlled flapping foils," Applied Ocean Research **52**, 1–11 (2015).

[15] E. Bøckmann and S. Steen, "The effect of a fixed foil on ship propulsion and motions," in *Proceedings of the Third International Symposium on Marine Propulsors smp*, Vol. 13 (2013) pp. 553–561.

[16] F. F. Siala, K. Kamrani Fard, and J. A. Liburdy, "Experimental study of inertia-based passive flexibility of a heaving and pitching airfoil operating in the energy harvesting regime," Physics of Fluids **32** (2020), 10.1063/1.5119700.

[17] J. R. Xing, D. Stagonas, P. Hart, C. C. Zhang, J. H. Yang, and L. Yang, "Wave induced thrust on a submerged hydrofoil: pitch stiffness effects," arXiv preprint arXiv:2209.05551 (2022), 10.48550/arXiv.2209.05551.

[18] J. Wang, S. Santhosh, O. Colomés, M. Capaldo, and L. Yang, "Experimental study of dynamic response of passive flapping hydrofoil in regular wave," Physics of Fluids **35** (2023), 10.1063/5.0157890.

[19] E. Bøckmann and S. Steen, "Experiments with actively pitch-controlled and spring-loaded oscillating foils," Applied Ocean Research **48**, 227–235 (2014).

[20] E. Filippas and K. Belibassakis, "A nonlinear time-domain bem for the performance of 3d flapping-wing thrusters in directional waves," Ocean Engineering **245**, 110157 (2022).

[21] S.-W. Huang, T.-L. Wu, Y.-T. Hsu, J.-H. Guo, J.-F. Tsai, and F.-C. Chiu, "Effective energy-saving device of eco-ship by using wave propulsion," in *2016 Techno-Ocean (Techno-Ocean)* (IEEE, 2016) pp. 566–570.

[22] E. Bøckmann, A. Yrke, and S. Steen, "Fuel savings for a general cargo ship employing retractable bow foils," Applied Ocean Research **76**, 1–10 (2018).

[23] Y. Zhang, L. Xu, Z. Ding, and M. Hu, "Wave propulsion and sea-keeping enhancement for ships in rough sea condition by flapping foils," Ocean Engineering **266**, 112802 (2022).

[24] K. Niklas and H. Pruszko, "The retrofitting of ships by applying retractable bow hydrofoils: a case study," Journal of Ocean Engineering and Marine Energy **9**, 767–788 (2023).

[25] Y. Zhang, L. Xu, and Y. Zhou, "A wave foil with passive angle of attack adjustment for wave energy extraction for ships," Ocean Engineering **246**, 110627 (2022).

[26] W. Tian, A. Bodling, H. Liu, J. C. Wu, G. He, and H. Hu, "An experimental study of the effects of pitch-pivot-point location on the propulsion performance of a pitching airfoil," Journal of fluids and structures **60**, 130–142 (2016).

[27] A. Mackowski and C. Williamson, "Effect of pivot location and passive heave on propulsion from a pitching airfoil," Physical Review Fluids **2**, 013101 (2017).

[28] Y. Zhang, Y. Feng, W. Chen, and F. Gao, "Effect of pivot location on the semi-active flapping hydrofoil propulsion for wave glider from wave energy extraction," Energy **255**, 124491 (2022).

[29] Z. Wang, L. Du, J. Zhao, and X. Sun, "Structural response and energy extraction of a fully passive flapping foil," Journal of Fluids and Structures **72**, 96–113 (2017).

[30] Y. Wang, X. Sun, D. Huang, and Z. Zheng, "Numerical investigation on energy extraction of flapping hydrofoils with different series foil shapes," Energy **112**, 1153–1168 (2016).

[31] J. M. Kelly, M. S. U. Khalid, P. Han, and H. Dong, "Geometric characteristics of flapping foils for enhanced propulsive efficiency," Journal of Fluids Engineering **145**, 061104 (2023).

[32] M. Soltani and A. Bakhshalipour, "Effect of amplitude and mean angle-of-attack on the boundary layer of an oscillating aerofoil," The Aeronautical Journal **112**, 705–713 (2008).

[33] L. Schouveiler, F. Hover, and M. Triantafyllou, "Performance of flapping foil propulsion," Journal of fluids and structures **20**, 949–959 (2005).

[34] P. Liu, Y. Liu, S. Huang, J. Zhao, and Y. Su, "Effects of regular waves on propulsion performance of flexible flapping foil," Applied Sciences **8**, 934 (2018).

[35] D. GL-OS-E301, "Offshore standard - position mooring (dnvgl-os- e301)," Edition July 2017 (2017).

[36] R. Cao, E. Padilla, and A. Callaghan, "The influence of bandwidth on the energetics of intermediate to deep water laboratory breaking waves," Journal of Fluid Mechanics **971**, A11 (2023).

[37] M. Triantafyllou, G. Triantafyllou, and R. Gopalkrishnan, "Wake mechanics for thrust generation in oscillating foils," Physics of Fluids A: Fluid Dynamics **3**, 2835–2837 (1991).